# Apolipoprotein E and Antioxidants Have Different Mechanisms of Inhibiting Alzheimer's β-Amyloid Fibril Formation in Vitro†

Hironobu Naiki,*,‡ Kazuhiro Hasegawa,§ Itaru Yamaguchi,|| Hideki Nakamura,|| Fumitake Gejyo,|| and Kazuya Nakakuki‡

*Departments of Pathology and of Clinical and Laboratory Medicine, Fukui Medical University, Fukui 910-1193, Japan, and Department of Biosystem Science, Graduate School of Science and Technology, Niigata University, Niigata 950-2181, Japan*

*Received March 11, 1998; Revised Manuscript Received September 22, 1998*

ABSTRACT: We compared the mechanisms of apolipoprotein E- (apoE-) and antioxidant- (AO-) mediated inhibition of β-amyloid fibril (fAβ) formation in vitro, based on a nucleation-dependent polymerization model using fluorescence spectroscopy with thioflavin T. We first applied a kinetic plot to transform a sigmoidal time-course curve of fAβ formation from freshly prepared amyloid β-peptides (Aβ) into a straight line. Mathematical treatment of this plot demonstrated that the above-described sigmoidal curve is a logistic curve and provided us with a kinetic parameter $t_{1/2}$, the time when the rate of fAβ formation is maximum. $t_{1/2}$ of β-amyloids (Aβ) (1−42) and (1−40) were 18.7 ± 1.7 min and 6.3 ± 0.2 h, respectively (mean ± SD, $n = 3$) and were independent of the initial Aβ concentration examined. Although apoE extended $t_{1/2}$ of both Aβs in a dose-dependent manner, AO did not. On the other hand, the final amount of fAβ formed was decreased by both apoE and AO dose-dependently. We then analyzed the effect of apoE and AO on the extension reaction of fAβ, based on a first-order kinetic model. Although apoE extended the time to proceed to equilibrium in a dose-dependent manner, AO did not. On the other hand, both apoE and AO dose-dependently decreased the final amount of fAβ formed. These results indicate that apoE and AO inhibit fAβ formation in vitro by different mechanisms and suggest the existence of multiple pharmacological targets for the prevention of fAβ formation.

Recently, we and other groups proposed a nucleation-dependent polymerization model to explain the mechanisms of β-amyloid fibril (fAβ)[1] formation in vitro (*1*−*4*). This model consists of two phases, i.e., nucleation and extension phases. Nucleus formation requires a series of association steps of monomers that are thermodynamically unfavorable, representing the rate-limiting step in amyloid fibril formation. Once the nucleus (*n*-mer) has been formed, further addition of monomers becomes thermodynamically favorable, resulting in a rapid extension of amyloid fibrils. We and other groups have independently developed a first-order kinetic model of fAβ extension in vitro and confirmed that the extension of fAβ proceeds via the consecutive association of amyloid β-peptides (Aβ) onto the ends of existing fibrils (*2*−*5*). Although this model is based on the assumption that Aβ are monomeric in the reaction mixture, stable Aβ dimers suggested by Walsh et al. (*6*) would also be consistent with this model. A characteristic sigmoidal time-course curve of fAβ formation from Aβ at a physiological pH is widely believed to represent the essence of a nucleation-dependent polymerization model; i.e., an initial lag phase represents the thermodynamically unfavorable nucleus formation (*1, 7*). However, no convincing kinetic models to explain the sigmoidality of the curve have been reported.

Apolipoprotein E (apoE) appears to play a central role in the pathogenesis of Alzheimer's disease (AD) (*8, 9*). Although many research groups have extensively examined the effect of apoE on fAβ formation in vitro, the results are somewhat conflicting. Some groups reported that apoE promoted and accelerated fAβ formation from Aβ in vitro (*10, 11*). However, other groups reported that apoE inhibited fAβ formation in vitro, based on a nucleation-dependent polymerization model (*7, 12, 13*). We showed that apoE has biphasic effects on fAβ formation in vitro, i.e., at low concentrations of β-amyloid(1−40) [Aβ(1−40)] (50 μM), a dose-dependent inhibitory effect of apoE on fAβ formation in vitro, while at high concentrations of Aβ(1−40) (300 μM), apoE shifted the time-course curves of fAβ formation upward (*7*). Several experiments have suggested that the upward shift of time-course curves by apoE observed at high concentrations of Aβ(1−40) may be largely due to the formation of apoE−Aβ(1−40) coaggregates and not to the promotion of fAβ formation (*7, 14, 15*).

† This research was supported in part by Grants-in-Aid 08670242 and 10670198 for Scientific Research (C) from the Ministry of Education, Science, Sports and Culture of Japan and by a grant from Ono Pharmaceutical Co., Ltd.

* Corresponding author. Tel. 081-776-61-8320; FAX 081-776-61-8123; E-mail naiki@fmsrsa.fukui-med.ac.jp.

‡ Department of Pathology, Fukui Medical University.

§ Department of Biosystem Science, Graduate School of Science and Technology, Niigata University.

|| Department of Clinical and Laboratory Medicine, Fukui Medical University.

[1] Abbreviations: Aβ, amyloid β-peptides; Aβ(1−40), β-amyloid-(1−40); Aβ(1−42), β-amyloid(1−42); AD, Alzheimer's disease; AO, antioxidants; apoE, apolipoprotein E; $\alpha_1$-MG, $\alpha_1$-microglobulin, DMSO, dimethyl sulfoxide; fAβ, β-amyloid fibrils; fAβ(1−40), β-amyloid fibrils formed from β-amyloid(1−40); fAβ(1−42), β-amyloid fibrils formed from β-amyloid(1−42); NDGA, nordihydroguaiaretic acid; RIF, rifampicin; ThT, thioflavin T.

10.1021/bi980550y CCC: $15.00 
Published on Web 11/26/1998

Increased oxidative stress may have a role in the pathogenesis of AD (*16*). Hensley et al. (*17*) showed that reactive oxygen species are generated by A$\beta$ fragments during cell-free incubation. Tomiyama et al. (*18, 19*) reported that rifampicin (RIF) and related agents inhibit A$\beta$ aggregation and neurotoxicity in a concentration-dependent manner. They also showed that the inhibitory activities of these agents are correlated with their radical-scavenging ability on hydroxyl free radicals. Ando et al. (*20*) showed that lipid peroxidation via free radical injury occurs in amyloid deposits of some types of systemic human amyloidosis. These findings strongly suggest that free radicals play an important role in the amyloid formation process.

Here, we characterize the kinetic properties of fA$\beta$ formation from fresh A$\beta$ at a physiological pH. We show that fA$\beta$ formation from $\beta$-amyloid(1−42) [A$\beta$(1−42)] and A$\beta$(1−40) proceeds by the same nucleation-dependent polymerization mechanism. A$\beta$(1−42) and A$\beta$(1−40) are the two major A$\beta$ forms found in amyloid deposits of AD brains (*21, 22*). On the basis of this model, we then compare the mechanisms of apoE- and antioxidant- (AO-) mediated inhibition of fA$\beta$ formation in vitro.

## EXPERIMENTAL PROCEDURES

*Preparation of A$\beta$ and fA$\beta$ Solutions.* A$\beta$(1−42) (lot number 511908, Bachem AG, Bubendorf, Switzerland) was dissolved by brief vortexing in ice-cold 0.1% ammonia solution at a concentration of about 250 $\mu$M (1.1 mg/mL) in a 4 °C room. Although the solution was clear, short fibrils were observed by electron microscopy (data not shown). Significant thioflavin T (ThT) fluorescence was also detected by fluorescence spectroscopy. To remove these fibrils, the solution (0.8 mL) was applied to polycarbonate tubes (size 11 × 34 mm, code number 343778; Beckman, Palo Alto, CA), and ultracentrifuged at $10^5g$, for 3 h, at 4 °C, using a Beckman Optima TLX tabletop ultracentrifuge and a Beckman TLA-120.2 fixed-angle rotor. Although no visible pellets were formed after ultracentrifugation, the ThT fluorescence was collected to the bottom quarter fraction and no significant fluorescence was detected in the upper three-quarter fraction. By electron microscopy, no fibrillar components were observed in the upper three-quarter fraction. Therefore, the upper three-quarter fraction was collected by careful aspiration and stored at −80 °C before assaying [fresh A$\beta$(1−42) solution]. The protein concentration of this fraction, as measured by the method described below, was similar to that of the whole solution before ultracentrifugation. A$\beta$-(1−40) (lot number 515587, Bachem AG, Bubendorf, Switzerland) was dissolved by brief vortexing in ice-cold distilled water at a concentration of about 500 $\mu$M (2.2 mg/mL) in a 4 °C room and stored at −80 °C before assaying [fresh A$\beta$(1−40) solution]. Unless otherwise noted, the above-described two A$\beta$ lots were used throughout the experiment. A$\beta$(1−42) from a different lot (lot number 511907, Bachem AG, Bubendorf, Switzerland) and a different vendor (lot number L00962, Alexis Biochemicals Co., San Diego, CA) and A$\beta$(1−40) from different lots (lot numbers WM365, 510313, and 515587, Bachem AG, Bubendorf, Switzerland) were also treated as described above.

fA$\beta$ [fA$\beta$(1−42)] was formed from the above-described fresh A$\beta$(1−42) solution. The reaction mixture in an Eppendorf tube was 950 $\mu$L and contained 25 $\mu$M A$\beta$(1−42), 50 mM phosphate buffer, pH 7.5, and 100 mM NaCl. After being briefly vortexed, the mixture was incubated at 37 °C for 6 h for polymerization reactions. The reaction tubes were not agitated during the reaction. After incubation, the mixture was centrifuged at 4 °C for 3 h at 1.5 × $10^4$ rpm, using a high-speed refrigerated microcentrifuge (MRX-150, Tomy, Tokyo, Japan). More than 95% of fA$\beta$(1−42) had precipitated as measured by the fluorescence of ThT. The pellet was resuspended in 50 mM phosphate buffer, pH 7.5, 100 mM NaCl, and 0.05% $NaN_3$ in an Eppendorf tube, sonicated on ice with 15 intermittent pulses (pulse 0.6 s, interval 0.4 s, output level 2) from an ultrasonic disruptor (UD-201, Tomy, Tokyo, Japan) equipped with a microtip (TP-030, Tomy, Tokyo, Japan), and stored at 4 °C before assaying. Another type of fA$\beta$ [fA$\beta$(1−40)] was formed from the above-described fresh A$\beta$(1−40) solution. The reaction mixture was 600 $\mu$L and contained 50 $\mu$M A$\beta$(1−40), 50 mM phosphate buffer, pH 7.5, and 100 mM NaCl. After incubation at 37 °C for 24 h, the mixture was centrifuged at 4 °C for 3 h at 1.5 × $10^4$ rpm. fA$\beta$(1−40) had precipitated completely as measured by the fluorescence of ThT. The pellet was resuspended in 50 mM phosphate buffer, pH 7.5, 100 mM NaCl, and 0.05% $NaN_3$, sonicated as described above and stored at 4 °C before assaying.

*Fluorescence Spectroscopy.* All studies were performed essentially as described elsewhere (*2*), on a Hitachi F-3010 fluorescence spectrophotometer. Optimum fluorescence measurements of fA$\beta$ were obtained at the excitation and emission wavelengths of 446 and 490 nm, respectively, with the reaction mixture containing 5 $\mu$M ThT (Wako Pure Chemical Industries, Ltd., Osaka, Japan) and 50 mM of glycine-NaOH buffer, pH 8.5 (*2*). Fluorescence was measured immediately after the mixture was made and was averaged for the initial 5 s.

*Polymerization Assay.* Reaction mixtures were prepared on ice at 4 °C, with neither polymerization nor depolymerization of fA$\beta$ being observed by fluorometric analysis. Distilled water was put into a tube. Then 500 mM phosphate buffer, pH 7.5, was added to yield a final buffer concentration of 50 mM, and 5 M NaCl was added to a final concentration of 100 mM. Fresh A$\beta$ solutions were added to yield final A$\beta$ concentrations of 5, 12.5, 25, and 30 $\mu$M [A$\beta$(1−42)] or 10, 25, and 50 $\mu$M [A$\beta$(1−40)]. Recombinant human apoE3 (lot number LEE7309, Wako Pure Chemical Industries, Ltd., Osaka, Japan) dissolved in 50 mM phosphate buffer, pH 7.5, and 100 mM NaCl, was added to yield final apoE concentrations of 0, 50, 100, and 250 nM and 1 $\mu$M. Before addition to the mixture, recombinant apoE3 was treated as described previously (*7*). In some experiments, human $\alpha_1$-microglobulin ($\alpha_1$-MG) [lot number 065(501), DAKO A/S, Glostrup, Denmark] dissolved in 15 mM $NaN_3$ at a concentration of 554 mg/L (20.7 $\mu$M) was added as a negative control of apoE, to a final $\alpha_1$-MG concentration of 100 nM. Nordihydroguaiaretic acid (NDGA) (Sigma Chemical Co., St. Louis, MO) and RIF (Sigma Chemical Co., St. Louis, MO) dissolved in dimethyl sulfoxide (DMSO) (Nacalai Tesque, Inc., Kyoto, Japan) at concentrations of 1 and 3 mM (NDGA) and 10 mM (RIF) were added to final concentrations of 10, 30, and 100 $\mu$M, respectively. The negative control mixtures contained 1% DMSO. Finally, fA$\beta$ solution was added to yield a final fA$\beta$ concentration of 15

ng of protein/$\mu$L [fA$\beta$(1−42)] or 50 ng/$\mu$L [fA$\beta$(1−40)].

After brief vortexing of the mixture, 30 $\mu$L aliquots were put into oil-free PCR tubes (size 0.5 mL, code number 9046, Takara Shuzo Co. Ltd., Otsu, Japan). The reaction tubes were then transferred into a DNA thermal cycler (PJ480, Perkin-Elmer Cetus, Emeryville, CA). Starting at 4 °C, the plate temperature was elevated at maximal speed to 37 °C. Incubation times ranged between 0 and 12 h (as indicated in each figure), and the reaction was stopped by placing the tubes on ice. The reaction tubes were not agitated during the reaction. From each reaction tube, triplicate 5-$\mu$L aliquots were removed and subjected to fluorescence spectroscopy, and the mean of each triplicate was determined.

*Electron Microscopy and Polarized Light Microscopy.* Reaction mixtures were spread on carbon-coated grids, negatively stained with 1% phosphotungstic acid, pH 7.0 and examined under a Hitachi H-7000 electron microscope with an acceleration voltage of 75 kV.

Part of the reaction mixtures were centrifuged at 4 °C for 90 min at $1.5 \times 10^4$ rpm. Pellets were spread on glass slides, dried overnight in an incubator set at 37 °C, stained with Congo red, and examined under a polarized light microscope to check for orange-green birefringence.

*Other Analytical Procedures.* Protein concentrations of the A$\beta$ and fA$\beta$ solutions were determined by the method of Bradford (*23*) with a protein assay kit (500−0001, Bio-Rad Laboratories, Inc., Hercules, CA). Throughout this study, the A$\beta$(1−40) solution quantified by amino acid analysis was used as the standard. Equal amounts of A$\beta$(1−42) and A$\beta$-(1−40) quantified by amino acid analysis gave similar absorbance. Bovine $\gamma$-globulin was used for the quantification of apoE solutions. Linear least-squares fitting was performed using CA-Cricket Graph III (version 1.5.3J, Computer Associates International Inc., Islandia, NY) and a Macintosh computer (Power Macintosh 8500/180).

## RESULTS

*Formation of fA$\beta$.* fA$\beta$(1−40) assumed the nonbranched, helical filament structure of approximately 7 nm in width and exhibited a helical periodicity of approximately 120 nm (*2*). They also showed typical orange-green birefringence under polarized light after Congo red staining (*2*). As shown in Figure 1, two types of amyloid fibrils could be formed from the fresh A$\beta$(1−42) solution. Type A fibrils assumed the nonbranched filament structure of approximately 8 nm width. Although the helical structure was observed in some type A fibrils, it was not as distinct as in the case of fA$\beta$-(1−40). Type B fibrils assumed the nonbranched filament structure of approximately 12 nm width and exhibited no helical structure. Seilheimer et al. (*24*) observed similar heterogeneity in the structure of fA$\beta$(1−42) formed in vitro. When fA$\beta$(1−42) were stained with Congo red, they showed typical orange-green birefringence under polarized light (data not shown).

*Kinetics of fA$\beta$ Formation from Fresh A$\beta$.* As shown in Figure 2A, when fresh A$\beta$(1−42) (lot number 511908) was incubated at 37 °C, the fluorescence of ThT followed a characteristic sigmoidal curve. The final equilibrium level increased, in a concentration-dependent manner, with A$\beta$-(1−42). This curve is consistent with a nucleation-dependent polymerization model (*1, 7, 12*).

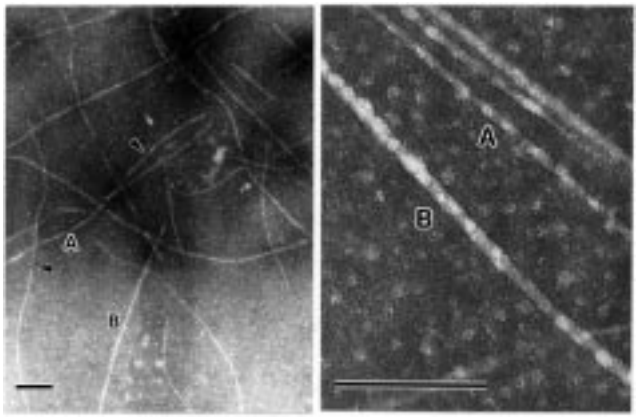


FIGURE 1: Electron micrograph of fA$\beta$(1−42). The reaction mixture containing 25 $\mu$M A$\beta$(1−42), 50 mM phosphate buffer, pH 7.5, and 100 mM NaCl was incubated at 37 °C for 60 min and then prepared for electron microscopy as described under Experimental Procedures. Note that type A (A) and type B fibrils (B) with diameters of approximately 8 and 12 nm, respectively, were formed. In some type A fibrils, the helical structure with nodes (arrowheads) was observed. The bar indicates a length of 100 nm.

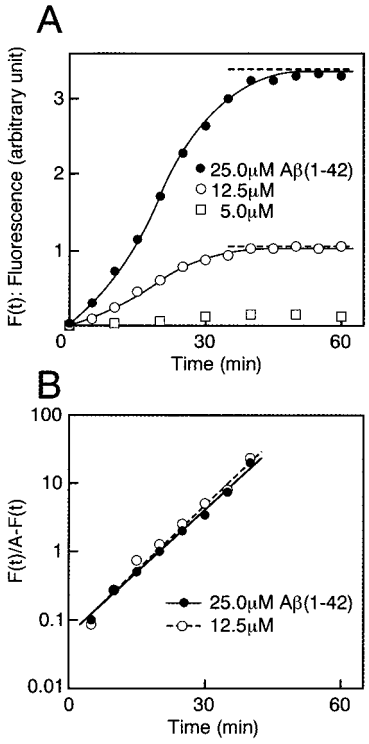


FIGURE 2: Kinetics of fA$\beta$(1−42) formation from fresh A$\beta$(1−42). (A) Time course of the fluorescence after the initiation of the reaction. $F(t)$ represents the fluorescence as a function of time. The reaction mixture contained 50 mM phosphate buffer, pH 7.5, 100 mM NaCl, and 5 (□), 12.5 (○), or 25 $\mu$M (●) A$\beta$(1−42). The reaction was initiated by shifting the temperature to 37 °C, as described under Experimental Procedures. At each incubation time (0−60 min), the reaction of the corresponding tube was stopped and analyzed by fluorescence spectroscopy as described under Experimental Procedures. (B) Semilogarithmic plots of the value $F(t)/A - F(t)$ versus incubation time. $A$ is tentatively determined as $F(\infty)$ and shown as a broken line on each sigmoidal curve. Linear least-squares fitting was performed for each straight line ($r = 0.993$ and 0.998 for ○ and ●, respectively). $t_{1/2}$ for ○ and ● was calculated to be 19.1 and 20.3 min, respectively. This is a representative pattern of three independent experiments.

Plotting the fluorescence data as common logarithms, shown in Figure 2B, gives two linear semilogarithmical plots.

Interpretation of these plots yields

$$\log\left[\frac{F(t)}{A - F(t)}\right] = at + b \quad (1)$$

where $t$ is the reaction time, $F(t)$ is the fluorescence as a function of time, $A$ is tentatively determined as $F(\infty)$, and $a$ and $b$ are the slope and the $y$-intercept of each straight line, respectively. Differentiating eq 1 by $t$ and subsequent rearrangement yields

$$F'(t) = BF(t)[A - F(t)] \quad (2)$$

where $B = (a \ln 10)/A$, and $F'(t)$ represents the rate of fluorescence increase at a given time.

Equation 2 is a logistic differential equation and clearly shows that the above-described sigmoidal curve is a logistic curve (*25*). When $F(t) = A/2$, $F(t)/[A - F(t)] = 1$. Moreover, from eq 2, $F'(t)$ reaches its maximum, $(aA \ln 10)/4$. Therefore, from the straight lines shown in Figure 2B, we obtain the time when $F'(t)$ is maximum. We describe this time point as $t_{1/2}$. $t_{1/2}$ at the initial A$\beta$(1−42) concentration of 25 $\mu$M was 18.7 ± 1.7 min (mean ± SD, $n = 3$). $t_{1/2}$ was similar regardless of the initial A$\beta$(1−42) concentrations examined in this study. Similar sigmoidal curves and semilogarithmical plots were obtained in the case of fresh A$\beta$(1−40) (lot number 515587) (Figure 3). $t_{1/2}$ at the initial A$\beta$(1−40) concentration of 50 $\mu$M was 6.3 ± 0.2 h (mean ± SD, $n = 3$). To check the generality of eq 2, we examined the time-course curves of several other A$\beta$s [both A$\beta$(1−42) and A$\beta$(1−40)] from different lots and a different vendor (see Experimental Procedures). Although $t_{1/2}$ varied widely among different lots, eq 2 fit the data well in all of the time-course experiments (data not shown).

*Effects of ApoE and AO on the Kinetics of fA$\beta$ Formation from Fresh A$\beta$.* When 30 $\mu$M A$\beta$(1−42) was incubated with increasing concentrations of apoE3, a dose-dependent extension of the time to proceed to equilibrium, as well as a dose-dependent decrease in the final equilibrium level, was observed (Figure 4A). As shown in Figure 4B, eq 2 fit the fluorescence data completely regardless of the presence or absence of apoE3. Moreover, $t_{1/2}$ increased, in a dose-dependent manner, with apoE3. $\alpha_1$-MG (100 nM) had no significant effect on the above-described time-course experiments. Similar data were obtained in the case of fresh A$\beta$-(1−40) (*7*).

When 25 $\mu$M A$\beta$(1−42) was incubated with increasing concentrations of AO, the final equilibrium level showed a dose-dependent decrease (Figure 5A). NDGA exhibited much higher inhibitory activity than RIF. As shown in Figure 5B, eq 2 fit the fluorescence data completely regardless of the presence or absence of AO. In contrast to the case of apoE3, $t_{1/2}$ remained unchanged either with or without AO. Similar data were obtained for fresh A$\beta$(1−40) (data not shown).

*Effects of ApoE and AO on the Kinetics of fA$\beta$ Extension.* As shown in Figure 6A, when A$\beta$(1−42) was incubated with fA$\beta$(1−42) at 37 °C, the fluorescence of ThT increased without a lag phase and proceeded to equilibrium. The linear semilogarithmic plot shown in Figure 6B indicates that fA$\beta$-(1−42) extension can be explained by a first-order kinetic model (*2*). When fA$\beta$(1−42) and A$\beta$(1−42) were incubated with increasing concentrations of apoE3, a dose-dependent extension of the time to proceed to equilibrium, as well as a dose-dependent decrease in the final equilibrium level, was observed (Figure 6A). As shown in Figure 6B, a linear semilogarithmic plot was observed regardless of the presence or absence of apoE3. Moreover, the negative slope of the straight line increased, in a dose-dependent manner, with apoE3. Similar data were obtained for fA$\beta$(1−40) extension (*7*).

When fA$\beta$(1−42) and A$\beta$(1−42) were incubated with increasing concentrations of AO, the final equilibrium level decreased dose-dependently (Figure 7A). NDGA exhibited much higher inhibitory activity than RIF. As shown in Figure 7B, a linear semilogarithmical plot was observed regardless of the presence or absence of AO. In contrast to the case of apoE3, the slope of the straight line remained unchanged either with or without AO. Similar data were obtained in the case of fA$\beta$(1−40) extension (data not shown).

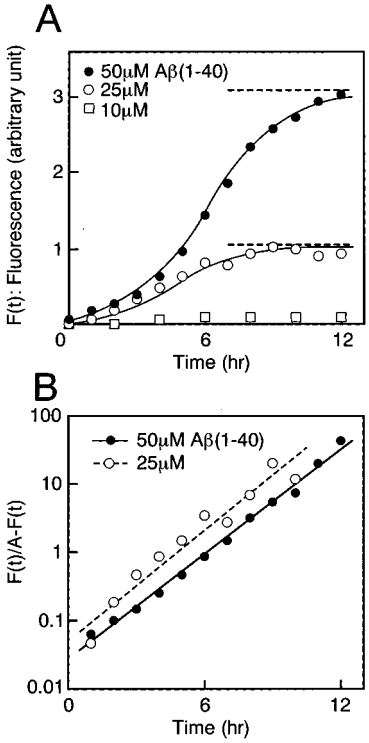


FIGURE 3: Kinetics of fA$\beta$(1−40) formation from fresh A$\beta$(1−40). (A) Time course of the fluorescence after the initiation of the reaction. $F(t)$ represents the fluorescence as a function of time. The reaction mixture contained 50 mM phosphate buffer, pH 7.5, 100 mM NaCl, and 10 (□), 25 (○), or 50 $\mu$M (●) A$\beta$(1−40). The reaction was initiated by shifting the temperature to 37 °C, as described under Experimental Procedures. At each incubation time (0−12 h), the reaction of the corresponding tube was stopped and analyzed by fluorescence spectroscopy as described under Experimental Procedures. (B) Semilogarithmic plots of the value $F(t)/A - F(t)$ versus incubation time. $A$ is tentatively determined as $F(\infty)$ and shown as a broken line on each sigmoidal curve. Linear least-squares fitting was performed for each straight line ($r = 0.970$ and 0.997 for ○ and ●, respectively). $t_{1/2}$ for ○ and ● was calculated to be 4.8 and 6.1 h, respectively. This is a representative pattern of three independent experiments.

## DISCUSSION

*Kinetic Properties of fA$\beta$ Formation from Freshly Prepared A$\beta$.* We used the fluorescence intensity of ThT as a measure of $f(t)$, which is the concentration of A$\beta$ constituting the whole fA$\beta$ as a function of time, based on the following: (1) The fluorescence intensity is linear with the increase

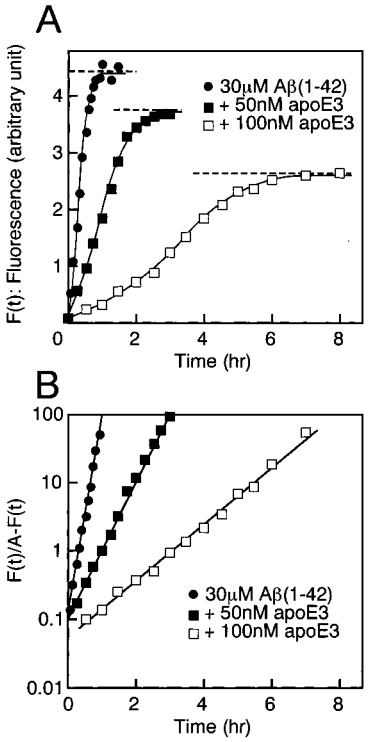


FIGURE 4: Effect of apoE on the kinetics of fA$\beta$(1−42) formation from fresh A$\beta$(1−42). (A) Time course of the fluorescence after the initiation of the reaction. $F(t)$ represents the fluorescence as a function of time. The reaction mixture contained 30 $\mu$M A$\beta$(1−42), 50 mM phosphate buffer, pH 7.5, 100 mM NaCl, and 0 (●), 50 (■), or 100 nM (□) apoE3. The reaction was initiated by shifting the temperature to 37 °C, as described under Experimental Procedures. At each incubation time (0−8 h), the reaction of the corresponding tube was stopped and analyzed by fluorescence spectroscopy as described under Experimental Procedures. (B) Semilogarithmic plots of the value $F(t)/A - F(t)$ versus incubation time. $A$ is tentatively determined as $F(\infty)$ and shown as a broken line on each sigmoidal curve. Linear least-squares fitting was performed for each straight line ($r$ = 0.998, 0.999, and 0.998 for ●, ■, and □, respectively). $t_{1/2}$ for ●, ■, and □ was calculated to be 20.1, 57.8, and 181.1 min, respectively. This is a representative pattern of three independent experiments.

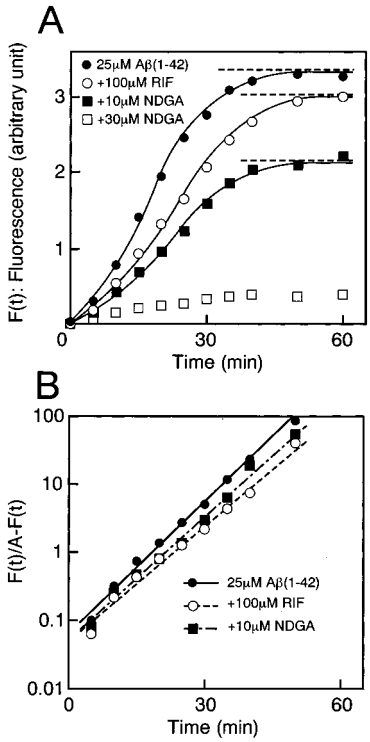


FIGURE 5: Effect of AO on the kinetics of fA$\beta$(1−42) formation from fresh A$\beta$(1−42). (A) Time course of the fluorescence after the initiation of the reaction. $F(t)$ represents the fluorescence as a function of time. The reaction mixture contained 25 $\mu$M A$\beta$(1−42), 50 mM phosphate buffer, pH 7.5, 100 mM NaCl, and 0 (●) or 100 $\mu$M (○) RIF or 10 (■) or 30 $\mu$M (□) NDGA. The reaction was initiated by shifting the temperature to 37 °C, as described under Experimental Procedures. At each incubation time (0−60 min), the reaction of the corresponding tube was stopped and analyzed by fluorescence spectroscopy as described under Experimental Procedures. (B) Semilogarithmic plots of the value $F(t)/A - F(t)$ versus incubation time. $A$ is tentatively determined as $F(\infty)$ and shown as a broken line on each sigmoidal curve. Linear least-squares fitting was performed for each straight line ($r$ = 0.997, 0.994, and 0.996 for ●, ○, and ■, respectively). $t_{1/2}$ for ●, ○, and ■ was calculated to be 18.7, 23.5, and 21.3 min, respectively. This is a representative pattern of three independent experiments.

in the protein concentration of amyloid fibrils (*2, 26 27*). (2) The fluorescence intensity is independent of the number concentration or the mean length of amyloid fibrils if the protein concentration of amyloid fibrils is constant (*2, 28*). (3) In the extension kinetics study where the number concentration of amyloid fibrils is constant, the increase in the average length of amyloid fibrils corresponds to the increase in the fluorescence intensity (*28*). At present, there is no proof that the signal response of ThT is constant among the different fibrillar structures formed from soluble A$\beta$ during fibrillogenesis, e.g., prenuclei, nuclei, short fibrils, long fibrils, and fibril bundles. In fact, some heterogeneity of fA$\beta$(1−42) was observed in the reaction mixture after proceeding to equilibrium (see Figure 1). However, for the simplicity of the model, we assume that the fluorescence intensity of ThT is proportional to $f(t)$.

From eqs 1 and 2, we obtain

$$f'(t) = Bf(t)[A - f(t)] \quad (3)$$

where $A = f(\infty)$, $B$ is a constant (described above), and $f'(t)$ represents the rate of increase in the whole fA$\beta$ at a given time.

We showed that fA$\beta$ formation from fresh A$\beta$ follows a logistic equation (see eq 2). Various biological phenomena can be explained by a logistic equation (*25*): e.g., growth processes of bacteria, yeast, and plants, aging/survival data for various organisms, and the autocatalytic reaction of trypsin that converts trypsinogen into trypsin. We used this equation simply to compare the shape of sigmoidal curves. In the process of fA$\beta$ formation from fresh A$\beta$, the shape of each sigmoidal curve is determined by two parameters, i.e., $t_{1/2}$ and the final equilibrium level. From eqs 2 and 3, $t_{1/2}$ is the time when $f'(t)$ is maximum. $t_{1/2}$ of 25 $\mu$M A$\beta$(1−42) and 50 $\mu$M A$\beta$(1−40) was 18.7 ± 1.7 min and 6.3 ± 0.2 h, respectively (see Figures 2 and 3). On the other hand, when equal concentrations of A$\beta$(1−42) and A$\beta$(1−40) were incubated with the corresponding fA$\beta$s (seeding experiments), the extension reaction of fA$\beta$s followed a first-order kinetic model proceeding to equilibrium at a similar rate and within 30 min in both cases (see Figure 6 and ref *7*). These results may indicate that a nucleation-dependent polymerization process really occurs in fA$\beta$ formation in vitro: i.e., the entire process of fA$\beta$ formation from fresh A$\beta$ is governed by the nucleation process. Therefore, it may be

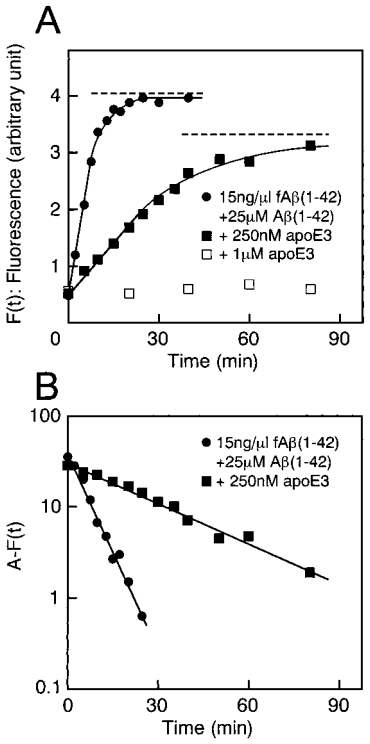


FIGURE 6: Effect of apoE on the kinetics of fA$\beta$(1−42) extension. (A) Time course of the fluorescence after the initiation of the reaction. $F(t)$ represents the fluorescence as a function of time. The reaction mixture contained 15 ng/$\mu$L fA$\beta$(1−42), 25 $\mu$M A$\beta$(1−42), 50 mM phosphate buffer, pH 7.5, 100 mM NaCl, and 0 (●), 250 nM (■), or 1 $\mu$M (□) apoE3. The reaction was initiated by shifting the temperature to 37 °C, as described under Experimental Procedures. At each incubation time (0−90 min), the reaction of the corresponding tube was stopped and analyzed by fluorescence spectroscopy as described under Experimental Procedures. (B) Semilogarithmic plots of the difference $A - F(t)$ versus incubation time. $A$ is tentatively determined as $F(\infty)$ and shown as a broken line on each hyperbolic curve. Linear least-squares fitting was performed for each straight line ($r = -0.995$ and $-0.991$ for ● and ■, respectively). This is a representative pattern of three independent experiments.

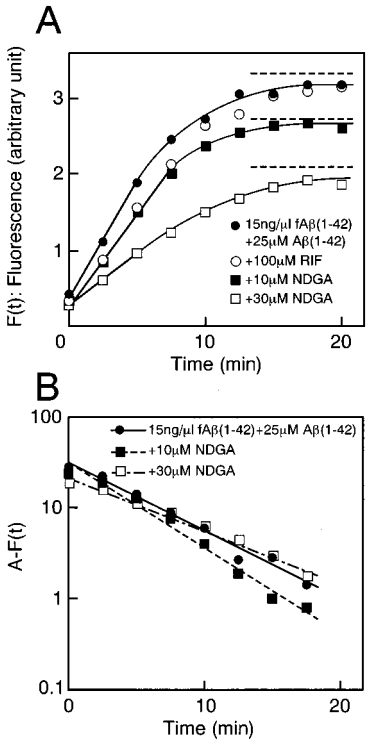


FIGURE 7: Effect of AO on the kinetics of fA$\beta$(1−42) extension. (A) Time course of the fluorescence after the initiation of the reaction. $F(t)$ represents the fluorescence as a function of time. The reaction mixture contained 15 ng/$\mu$L fA$\beta$(1−42), 25 $\mu$M A$\beta$(1−42), 50 mM phosphate buffer, pH 7.5, 100 mM NaCl, and 0 (●) or 100 $\mu$M (○) RIF or 10 (■) or 30 $\mu$M (□) NDGA. The reaction was initiated by shifting the temperature to 37 °C, as described under Experimental Procedures. At each incubation time (0−20 min), the reaction of the corresponding tube was stopped and analyzed by fluorescence spectroscopy as described under Experimental Procedures. (B) Semilogarithmic plots of the difference $A - F(t)$ versus incubation time. $A$ is tentatively determined as $F(\infty)$ and shown as a broken line on each hyperbolic curve. Linear least-squares fitting was performed for each straight line ($r = -0.992$ in all cases). This is a representative pattern of three independent experiments.

reasonable to use $t_{1/2}$ as an indicator of the potential of each A$\beta$ to form a nucleus. Comparison of $t_{1/2}$ of both A$\beta$s indicates that A$\beta$(1−42) has a much higher potential of spontaneous nucleus formation than A$\beta$(1−40).

We compared the kinetic properties of fA$\beta$ formation described in this article with those of actin polymerization. When G-actin is incubated under appropriate conditions, the polymerization kinetics of G-actin into F-actin follows a characteristic sigmoidal curve (*29, 30*). Polymerization kinetics is highly dependent on the initial G-actin concentration; i.e., the higher the initial concentration, the shorter the time proceeding to equilibrium (*30*). The set of experimental curves obtained at different actin concentrations (but under the same conditions) could be precisely fit by numerical integration of the following two equations describing a nucleation-dependent polymerization process (*30*). The nucleation rate is the rate of change in the number concentration of actin filaments and can be expressed as

$$\frac{dC}{dt} = k_n(A_1)^n \tag{4}$$

where $C$ is the number concentration of actin filaments, $k_n$ is a nucleation rate constant, $A_1$ is the concentration of G-actin, and $n$ is the number of actin molecules constituting the nucleus ($n = 3$ or 4). The polymerization rate ($dA_F/dt$) can be expressed as

$$\frac{dA_F}{dt} = k^+CA_1 - k^-C \tag{5}$$

where $A_F$ is the concentration of F-actin, $k^+$ is the sum of the rate constants for monomer addition at the two filament ends, and $k^-$ is the sum of the rate constants for monomer dissociation at the two filament ends. Equation 5 describes a first-order kinetic model: i.e., the extension of actin filaments proceeds via the consecutive association of G-actin onto the ends of existing filaments. We have proposed that this model could be generally applied for the extension of all types of amyloid fibrils in vitro (*2, 27, 28*). By use of eqs 4 and 5, the temporal relationship of nucleation kinetics to polymerization kinetics was calculated (*30*). The nucleation rate is maximum at $t = 0$. Nucleation precedes polymerization, as it must, but is not confined to the earliest portion of the sigmoidal polymerization curve. Not until 45% of G-actin is polymerized does nucleation reach 95% completion.

This model, especially the model of actin nucleation, cannot explain the kinetic properties of fA$\beta$ formation described in this article. Although characteristic sigmoidal curves were observed in the process of fA$\beta$ formation from fresh A$\beta$, the time proceeding to equilibrium remained unchanged regardless of the initial A$\beta$ concentration examined (see Figures 2 and 3, where $t_{1/2}$ was similar).

Lomakin et al. (*3*, *4*) performed quasielastic light scattering studies of fibrillogenesis of A$\beta$(1−40) in 0.1 M HCl, because in such a milieu, fibril growth was reproducible and sufficiently slow to allow detailed monitoring of the entire process of fibril growth. They used a calibration curve relating the hydrodynamic radius, $R_H$, of a monodisperse solution of rigid rods as a function of the fibril length, $L$, or the number of A$\beta$ monomers constituting each fibril, $p$. They suggested a kinetic model in which (i) fibrillogenesis requires a nucleation step, (ii) nuclei are produced by A$\beta$ micelles in addition to nuclei initially present, and (iii) fibril elongation occurs by irreversible binding of A$\beta$ monomers to the fibril ends. Their theory is similar in many points to the theory presented here, as well as the above-described model of actin nucleation and polymerization. First, their theory supports a nucleation-dependent polymerization model. They postulated micelles from which nuclei are spontaneously formed with rate constant $k_n$ provided that the A$\beta$ concentration exceeds the critical micellar concentration $c^*$. Second, their theory clearly indicates that fibril elongation can be explained by a first-order kinetic model: i.e., fibrils grow by binding monomers to fibril ends with the rate proportional to the concentration of free monomers. Third, their theory indicates that the total number concentration of A$\beta$ in fibrillar form, $N^{(1)}$ [corresponding to the above-described $f(t)$], changes as a result of both the creation of nuclei and the binding of monomers to the ends of each fibril. Despite these similarities, their theory concerning the nucleation kinetics cannot explain the concentration-dependent upward shift of the sigmoidal curves (see Figures 2 and 3). Their theory indicates that the rate of the increase in the total number of fibrils of all sizes, $\dot{N}^{(0)}$, is equal to $k_nM$, where $M$ is the number concentration of micelles. $M$ is linear to the $m_0$th power of the free A$\beta$ concentration, where $m_0$ is the number of A$\beta$ monomers in a micelle ($15 < m_0 < 70$). $\dot{N}^{(0)}$ is maximum at $t = 0$ and then gradually decreases with the decrease in $M$. As in the case of F-actin formation, if $\dot{N}^{(0)}$ is proportional to the $m_0$th power of the free A$\beta$ concentration, the time proceeding to equilibrium would decrease, in a concentration-dependent manner, with A$\beta$ (see Figures 2 and 3, where $t_{1/2}$ was similar).

We conclude that the data presented in this paper are not sufficient to propose a novel kinetic model of the nucleation process at a physiological pH. Therefore, we cannot evaluate the validity of eq 3 on the basis of a kinetic scheme. Some additional steps might exist prior to or associated with the nucleation process. One possible working hypothesis is the existence of a monomer activation step after the initiation of the reaction, where a conformational change might be induced in A$\beta$ prior to the association of A$\beta$ molecules with each other to form a nucleus. In this case, some lag time would be observed before the nucleation rate reaches its maximum. Clearly, more extensive studies combining fluorometric analysis with ThT with several other paradigms (e.g., quasielastic light scattering study, circular dichroism spectroscopy) are eagerly awaited to construct a novel scheme of the nucleation process at a physiological pH.

*Comparison of the Inhibitory Mechanisms of apoE and AO on fA$\beta$ Formation in Vitro.* ApoE may inhibit the extension of fA$\beta$ in vitro and extend the time to proceed to equilibrium by making a complex with A$\beta$, thus eliminating free A$\beta$ from the reaction mixture (*7*; see Figure 6). Thus, we hypothesized that apoE would inhibit the nucleus formation by making a complex with A$\beta$ and/or prenuclei. Actually, apoE3 extended $t_{1/2}$ in a dose-dependent manner (see Figure 4).

In sharp contrast to apoE, AO had no effect on $t_{1/2}$ or the time to proceed to equilibrium in the extension reaction (see Figures 5 and 7). Therefore, it is not likely that AO would inhibit fA$\beta$ formation by making a complex with A$\beta$ and/or prenuclei. Further studies are necessary to clarify the mechanisms by which antioxidants inhibit fA$\beta$ formation in vitro.

*Biological Significance.* ApoE has been suggested to play a protective role against the progression of AD. First, Masliah et al. (*31*) found the synaptic and neuronal alterations in the central nervous system of Apoe knockout mice during the aging process. In both the central and peripheral nervous systems, apoE appears to participate in cholesterol redistribution and the repair response to tissue injury (*8*, *32*). Second, Miyata and Smith (*33*) showed that apoE isoproteins (E2, E3, E4) have antioxidant and neuroprotective activities in cell culture, with E2 > E3 > E4. Thus, increased levels of oxidative stress in apoE knockout mice would be predicted to enhance fA$\beta$ deposition (*34*). Very recently, Bales et al. (*35*) crossed apoE knockout mice with transgenic mice overexpressing a human mutant amyloid-$\beta$ precursor protein gene (V717F) and found that lack of apoE markedly reduces fA$\beta$ deposition in a transgenic model of AD. Their data defy the above-described expectation and suggest that inhibition of fA$\beta$ deposition, suggested by several in vitro experiments (*7*, *12*, *13*), is not the major role of apoE in vivo. While we have no clear explanation for this discrepancy between in vitro and in vivo studies, high-affinity apoE−A$\beta$ complexes might be carried via a lipoprotein pathway to endosomal and lysosomal vesicles, which could be favorable for the initiation of fA$\beta$ formation in vivo (*36*).

Sano et al. (*37*) demonstrated that in AD patients with moderately severe impairment, treatment with selegiline or α-tocopherol (vitamin E) retards the progression of disease. Selegiline, a monoamine oxidase inhibitor, may act as an antioxidant, since it inhibits oxidative deamination, thereby reducing neuronal damage. α-Tocopherol, a free radical scavenger, has been shown to inhibit A$\beta$ aggregation in vitro (*19*), as well as inhibiting A$\beta$-induced death of a clone of PC12 cells (*38*). These findings strongly suggest not only that free radicals are involved in the pathogenesis of neuron death in AD but also that trapping of free radicals and prevention of their formation may be beneficial for the treatment of AD (*16*).

Comparison of the inhibitory effects of apoE and AO clearly indicates two pharmacological strategies that could be applied to inhibit or retard amyloid fibril formation in several kinds of human amyloidoses. We believe that the experimental system described in this article may prove useful in the development of nonpeptide inhibitors of amyloid fibril formation in vivo.

## ACKNOWLEDGMENT

We thank Dr. R. Seo, Ono Pharmaceutical Co., Ltd., for helpful experimental advice and C. Masuda, H. Okada, and N. Takimoto for excellent technical assistance.

## REFERENCES

1. Jarrett, J. T., and Lansbury, P. T., Jr. (1993) *Cell 73*, 1055−1058.
2. Naiki, H., and Nakakuki, K. (1996) *Lab. Invest. 74*, 374−383.
3. Lomakin, A., Chung, D. S., Benedek, G. B., Kirschner, D. A., and Teplow, D. B. (1996) *Proc. Natl. Acad. Sci. U.S.A. 93*, 1125−1129.
4. Lomakin, A., Teplow, D. B., Kirschner, D. A., and Benedek, G. B. (1997) *Proc. Natl. Acad. Sci. U.S.A. 94*, 7942−7947.
5. Esler, W. P., Stimson, E. R., Ghilardi, J. R., Vinters, H. V., Lee, J. P., Mantyh, P. W., and Maggio, J. E. (1996) *Biochemistry 35*, 749−757.
6. Walsh, D. M., Lomakin, A., Benedek, G. B., Condron, M. M., and Teplow, D. B. (1997) *J. Biol. Chem. 272*, 22364−22372.
7. Naiki, H., Gejyo, F., and Nakakuki, K. (1997) *Biochemistry 36*, 6243−6250.
8. Poirier, J. (1994) *Trends Neurosci. 17*, 525−530.
9. Castaño, E. M., Prelli, F. C., and Frangione, B. (1995) *Lab. Invest. 73*, 457−460.
10. Wisniewski, T., Castaño, E. M., Golabek, A., Vogel, T., and Frangione, B. (1994) *Am. J. Pathol. 145*, 1030−1035.
11. Ma, J., Yee, A., Brewer, H. B., Jr., Das, S., and Potter, H. (1994) *Nature 372*, 92−94.
12. Evans, K. C., Berger, E. P, Cho, C.-G., Weisgraber, K. H., and Lansbury, P. T., Jr. (1995) *Proc. Natl. Acad. Sci. U.S.A. 92*, 763−767.
13. Wood, S. J., Chan, W., and Wetzel, R. (1996) *Biochemistry 35*, 12623−12628.
14. Chan, W., Fornwald, J., Brawner, M., and Wetzel, R. (1996) *Biochemistry 35*, 7123−7130.
15. Wood, S. J., Chan, W., and Wetzel, R. (1996) *Chem. Biol. 3*, 949−956.
16. Markesbery, W. R. (1997) *Free Radic. Biol. Med. 23*, 134−147.
17. Hensley, K., Carney, J. M., Mattson, M. P., Aksenova, M., Harris, M., Wu, J. F., Floyd, R. A., and Butterfield, D. A. (1994) *Proc. Natl. Acad. Sci. U.S.A. 91*, 3270−3274.
18. Tomiyama, T., Asano, S., Suwa, Y., Morita, T., Kataoka, K., Mori, H., and Endo, N. (1994) *Biochem. Biophys. Res. Commun. 204*, 76−83.
19. Tomiyama, T., Shoji, A., Kataoka, K., Suwa, Y., Asano, S., Kaneko, H., and Endo, N. (1996) *J. Biol. Chem. 271*, 6839−6844.
20. Ando, Y., Nyhlin, N., Suhr, O., Holmgren, G., Uchida, K., Sahly, M. E., Yamashita, T., Terasaki, H., Nakamura, M., Uchino, M., and Ando, M. (1997) *Biochem. Biophys. Res. Commun. 232*, 497−502.
21. Roher, A. E., Lowenson, J. D., Clarke, S., Woods, A. S., Cotter, R. J., Gowing, E., and Ball, M. J. (1993) *Proc. Natl. Acad. Sci. U.S.A. 90*, 10836−10840.
22. Iwatsubo, T., Odaka, A., Suzuki, N., Mizusawa, H., Nukina, N., and Ihara, Y. (1994) *Neuron 13*, 45−53.
23. Bradford, M. M. (1976) *Anal. Biochem. 72*, 248−254.
24. Seilheimer, B., Bohrmann, B., Bondolfi, L., Müller, F., Stüber, D., and Döbeli, H. (1997) *J. Struct. Biol. 119*, 59−71.
25. Cerny, L. C., Stasiw, D. M., and Zuk, W. (1981) *Physiol. Chem. Phys. 13*, 221−230.
26. Naiki, H., Higuchi, K., Hosokawa, M., and Takeda, T. (1989) *Anal. Biochem. 177*, 244−249.
27. Naiki, H., Hashimoto, N., Suzuki, S., Kimura, H., Nakakuki, K., and Gejyo, F. (1997) *Amyloid: Int. J. Exp. Clin. Invest. 4*, 223−232.
28. Naiki, H., Higuchi, K., Nakakuki, K., and Takeda, T. (1991) *Lab. Invest. 65*, 104−110.
29. Pollard, T. D., and Cooper, J. A. (1986) *Annu. Rev. Biochem. 55*, 987−1035.
30. Tobacman, L. S., and Korn, E. D. (1983) *J. Biol. Chem. 258*, 3207−3214.
31. Masliah, E., Mallory, M., Ge, N., Alford, M., Veinbergs, I., and Roses, A. D. (1995) *Exp. Neurol. 136*, 107−122.
32. Mahley, R. W. (1988) *Science 240*, 622−630.
33. Miyata, M., and Smith, J. D. (1996) *Nat. Genet. 14*, 55−61.
34. Dyrks, T., Dyrks, E., Hartmann, T., Masters, C., and Beyreuther, K. (1992) *J. Biol. Chem. 267*, 18210−18217.
35. Bales, K. R., Verina, T., Dodel, R. C., Du, Y., Altstiel, L., Bender, M., Hyslop, P., Johnstone, E. M., Little, S. P., Cummins, D. J., Piccardo, P., Ghetti, B., and Paul, S. M. (1997) *Nat. Genet. 17*, 263−264.
36. Urmoneit, B., Prikulis, I., Wihl, G., D'Urso, D., Frank, R., Heeren, J., Beisiegel, U., and Prior, R. (1997) *Lab. Invest. 77*, 157−166.
37. Sano, M., Ernesto, C., Thomas, R. G., Klauber, M. R., Schafer, K., Grundman, M., Woodbury, P., Growdon, J., Cotman, C. W., Pfeiffer, E., Schneider, L. S., and Thal, L. J. (1997) *N. Engl. J. Med. 336*, 1216−1222.
38. Behl, C., Davis, J., Cole, G. M., and Schubert, D. (1992) *Biochem. Biophys. Res. Commun. 186*, 944−950.

BI980550Y